Reaction Rate Derivation for Plasmonic Chemistry and Experimental Verification

Author: Brian Olsen
Faculty Mentor: Professor Axel Scherer

1 Abstract

This research investigates the plasmon-enhanced photoswitching of azobenzene molecules, combining theoretical modeling and experimental nanofabrication. A non-equilibrium theoretical model is developed to predict the reaction rates of azobenzene under the influence of plasmonic fields, considering both weak and strong coupling regimes. Experimentally, we fabricate plasmonic nanostructures designed to generate high local field enhancements, and characterize their optical properties. Preliminary results demonstrate the successful fabrication of gold nanostructures with varying sizes and gaps. Future work will involve functionalizing these structures with azobenzene molecules and utilizing Raman spectroscopy to probe the switching dynamics under plasmonic excitation. The combination of theoretical modeling and experimental validation aims to provide a comprehensive understanding of plasmon-enhanced molecular switching, with potential applications in optical data storage, molecular electronics, and biosensing.

2 Introduction

Plasmonic nanostructures, capable of confining light to subwavelength scales due to the excitation of surface plasmon resonances (SPRs), have emerged as powerful tools for manipulating light-matter interactions [1]. The strong local field enhancements associated with SPRs offer exciting possibilities for controlling and enhancing various photochemical and photophysical processes at the nanoscale [2, 3]. One particularly interesting application lies in the field of molecular photoswitches, where plasmonic fields can be utilized to trigger and modulate the isomerization of photochromic molecules [4].

Azobenzene, a widely studied photochromic molecule, undergoes reversible isomerization between its *trans* and *cis* forms upon light irradiation [5]. This photoisomerization process leads to significant changes in the molecule's physical

and chemical properties, making azobenzene a promising candidate for applications in optical data storage, molecular electronics, and biosensing [6]. However, the efficiency of azobenzene photoswitching is often limited by the relatively low absorption cross-section of the molecule and the competing thermal relaxation pathways.

Plasmonic nanostructures offer a potential solution to overcome these limitations by providing intense and localized electromagnetic fields that can significantly enhance the light absorption and photoisomerization rates of azobenzene molecules. The precise control over the plasmonic field distribution and intensity through nanostructure design allows for the optimization of the photoswitching process [7]. Furthermore, the ability to tune the plasmonic resonance to match the absorption bands of azobenzene enables selective excitation and control of specific isomerization pathways [8].

In this research, we combine theoretical modeling and experimental nanofabrication to investigate the plasmon-enhanced photoswitching of azobenzene molecules. We develop a non-equilibrium theoretical model to predict the reaction rates of azobenzene under the influence of plasmonic fields. Experimentally, we fabricate plasmonic nanostructures designed to generate high local field enhancements and characterize their optical properties. The combination of theoretical modeling and experimental validation aims to provide a comprehensive understanding of plasmon-enhanced molecular switching, with potential implications for various technological applications.

3 Theoretical Framework

3.1 Reaction Rate Derivation for Unimolecular Plasmonic Systems

This was derived using the formalism in [9]. We consider a unimolecular system consisting of a single azobenzene molecule interacting with a plasmonic field. The system Hamiltonian is given by:

$$H_S = H_{mol} + H_{pl} + H_{int} \tag{1}$$

$$H_{mol} = \sum_{n=1}^{N_m} \left[\sum_{a_n} E_{na} |a_n\rangle\langle a_n| + \sum_{a_n \neq b_n} V_{a_n b_n} |a_n\rangle\langle b_n| \right] \tag{2}$$

$$H_{pl} = \sum_{k} \hbar\omega_{pl,k} b_k^\dagger b_k \tag{3}$$

$$H_{int} = -\sum_{nI} \left(\vec{\mu}_n \cdot \vec{g}_{n,k} b_k + \vec{\mu}_n \cdot \vec{g}_{n,k}^* b_k^\dagger \right) \tag{4}$$

Which for our unimolecular system of azobenzene (a molecule where the energy gap between molecular states S_1 and S_2 is large) provides the following

definitions for individual Hamiltonians:

$$H_{mol} = E_0 \left|S_0\right\rangle \left\langle S_0\right| + E_1 \left|S_1\right\rangle \left\langle S_1\right| + E_2 \left|S_2\right\rangle \left\langle S_2\right|$$

$$H_{\text{int}}^{ij,k} = \begin{cases} \mu_{S_i S_j} \cdot \mathbf{E}_{\text{pl,k}} \sqrt{n+1} & \text{if } m = n+1, m_{dir} = n_{dir} \\ \mu_{S_i S_j} \cdot \mathbf{E}_{\text{pl,k}} \sqrt{n} & \text{if } m = n-1, m_{dir} = n_{dir} \\ 0 & \text{otherwise} \end{cases}$$

$$H_{pl} = \sum_k \hbar \omega_{pl,k} b_k^\dagger b_k$$

with H_{pl} staying the same in this representation.

Now we many define a dividing surface function for our flux operator formalism where $h_{S_i S_j}$ is a projection operator onto the product state $|S_i\rangle$, constructed using the Heaviside step function $\theta(x)$:

$$h_{S_i S_j} = \sum_{n, n_{dir}} \theta((\frac{|S_i, n, n_{dir}\rangle - x_{ds})}{|B|} |S_i, n, n_{dir}\rangle\langle S_j, n, n_{dir}|)$$

$$\theta(x) = \begin{cases} 0, & \text{if } x < 0 \\ 1, & \text{if } x \geq 0 \end{cases}$$

And defining the flux operator as

$$F_{S_i S_j} = \frac{i}{\hbar}[H_S, h_{S_i S_j}] \tag{5}$$

This effectively captures the flux associated with transitions to the product state $|S_i\rangle$, with the Heaviside function acting as an implicit dividing surface, with $|S_i, n, n_{dir}\rangle$ being the index of the basis with those parameters (which is useful for the numerical implementations detailed in this report), and $|B|$ is the size (or length) of the constructed basis.

3.2 Flux Correlation Function and Reaction Rate

The flux correlation function is:

$$C_f(t) = \text{Tr}\left[F e^{-\frac{i}{\hbar} H_S t} \rho_r F e^{\frac{i}{\hbar} H_S t}\right]$$

and the reaction rate constant is:

$$k_{S_i S_j} = \int_0^\infty dt\, C_f^{S_i S_j}(t) \tag{6}$$

The flux correlation function is:

$$C_f(t) = \langle F(0) F(t) \rangle = \text{Tr}\left[F e^{-\frac{i}{\hbar} H_S t} \rho_r F e^{\frac{i}{\hbar} H_S t}\right] \tag{7}$$

where the density matrix, ρ_r, is given by:

$$\rho_r = \frac{1}{Z_r} e^{-\beta(H_{\text{mol}} + H_{\text{pl}} - Y)} \tag{8}$$

with the normalization constant:

$$Z_r = \text{Tr}\left[e^{-\beta(H_{\text{mol}} + H_{\text{pl}} - Y)}\right] \tag{9}$$

and the operator Y defined as:

$$Y = \sum_{\text{k modes}} \lim_{t\to\infty} e^{iH_{\text{sys}}t/\hbar} e^{-iH_{\text{pl}}t/\hbar} \left(\sum_{\text{n plasmons}} \hbar\omega b^\dagger b \right) \left(\lim_{t\to\infty} e^{iH_{\text{sys}}t/\hbar} e^{-iH_{\text{pl}}t/\hbar} \right)^{-1} \tag{10}$$

and the reaction rate constant is:

$$k = \int_0^\infty dt\, C_f(t) \tag{11}$$

In practice, this integral may be evaluated by a fourier transform Such that

$$k = \int_0^\infty C_f(t) e^{i\omega t} dt$$

And taking the zero frequency component. This leads to a more computationally efficient scaled average value of the correlation function giving us the same answer.

4 Experimental Methods

4.1 Nanostructure Fabrication

Plasmonic nanostructures were fabricated using electron beam lithography (EBL) followed by a lift-off process. A silicon substrate (Silicon Nitride or Si_3N_4) was coated with a layer of poly(methyl methacrylate) (PMMA) resist. EBL was then used to define the desired nanostructure patterns on the resist. The sample was then developed with a solution of original 1:3 MIBK:IPA ratio, but was replaced with simply IPA after features became increasingly more sensitive. Then, we ion-milled the samples via an Ar ion mill setup. After development, a thin film of gold was deposited onto the sample using a sputter coater. Then, we would leave the sample in a $13.56MHz$ O_2 plasma etcher. The remaining resist was removed using a lift-off process via pure acetone, leaving behind the gold nanostructures on the substrate. Finally, the structures were recrystallized via an oven reheating procedure at approximately a third of the temperature of Au.

The general settings were the following for the following steps in the fabrication process:

- **Electron Beam Lithography:** The beam current was $1.6nC/cm^2$, the acceleration voltage was $30kV$, and the magnification was $800x$ for most writes.
- **IPA/MIBK Development:** The process would usually last 15 seconds to 1 minute depending on the structure.
- **Ion Milling Treatment:** The process would usually last 15 seconds to 1 minute depending on the structure.
- **Au Sputtering Procedure:** We sputtered gold initially at 1 minute but decreased the value iteratively to reduce Au waste to around 30 seconds.
- O_2 **Plasma Etcher Cleaning Procedure:** We left the sample in the plasma etcher for approximately 15 minutes.
- **Acetone Liftoff Process:** The liftoff process including leaving the sample in acetone from 30 seconds to 1 minute, and rubbing the foil off with a cotton swab.
- **Au Recrystallization Procedure:** The samples were left in an oven at $330°C$ for 30 minutes under an approximately $500mL/min$ N_2 purge to reduce impurities.

Then we had to produce the monolayers on the samples. **Monolayer Preparation**

1. Prepare a solution of azobenzene in ethanol (concentration optimized for monolayer formation).
2. **Prepare Dilutions:**
   (a) For smaller volumes (e.g., dilutions in the 10^{-6} M range):
      i. Start by preparing a less dilute solution (e.g., 10^{-4} M) using the graduated cylinder and micropipette as described above.
      ii. Use the micropipette to take a small volume (e.g., 10 µL) of this solution and add it to another beaker containing the calculated volume of solvent (100 µL total) to achieve the next dilution (e.g., 10^{-5} M).
      iii. Repeat this process to reach desired final concentration (e.g., 10^{-6} M).
   (b) Label each beaker with the corresponding concentration.
3. Immerse the gold nanostructures in the azobenzene solution for a predetermined adsorption time (e.g., 1 hour)
4. Then seal in a plastic container and seal it very well under the hood.

4.2 Optical Characterization

The optical properties of the fabricated nanostructures were characterized using a Renishaw Raman spectrometer. The Raman Spectrometer was operated in the wavenumber range of 0 to 1600, with a $785nm$ excitation wavelength at $1mW$ using an exposure times of 10 seconds per scan, and a grating of $600l/mm$. The microscope was focused on a sample at $50x$ and was then used to get spectral image acquisitions of the samples for bulk sampling of the hotspot structures. Once the hotspots structures were found, we would background subtract the signals of the hotspot structures and their Raman Spectra with the parts of the sample that were just the wafer to produce the corresponding Raman Spectra in the results section.

5 Results and Discussion

5.1 Nanostructure Fabrication Results

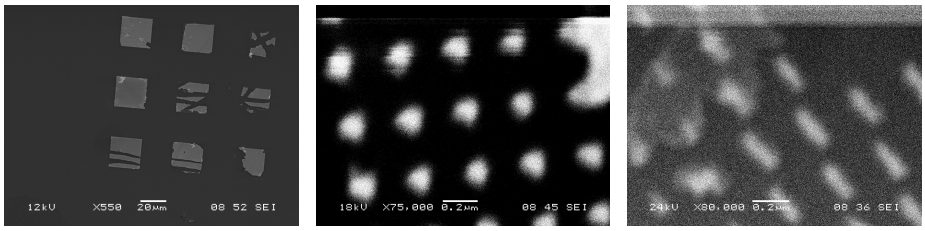

These are a few of the many variations of structures that we produced for this research project. The smallest dimensions that we achieved were around a gap size of around 50 nm controllably, with the feature sizes being of similar order. The first image is a map of the pattern that was made on the more macroscopic scale, and then the second and third images are the microscopic structures.

5.2 Optical Characterization

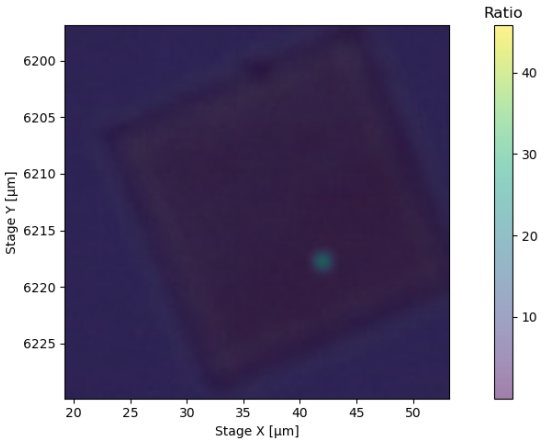

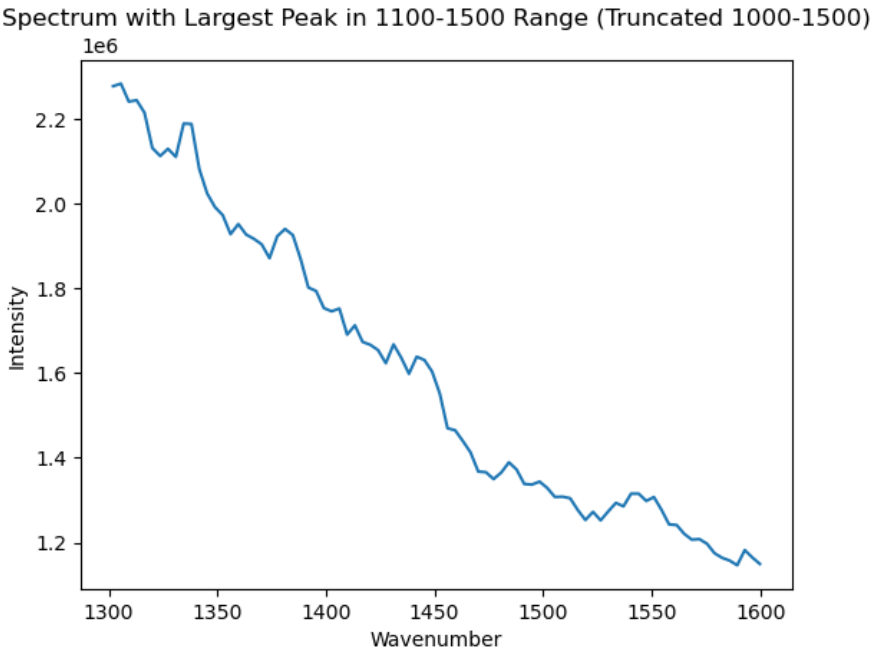

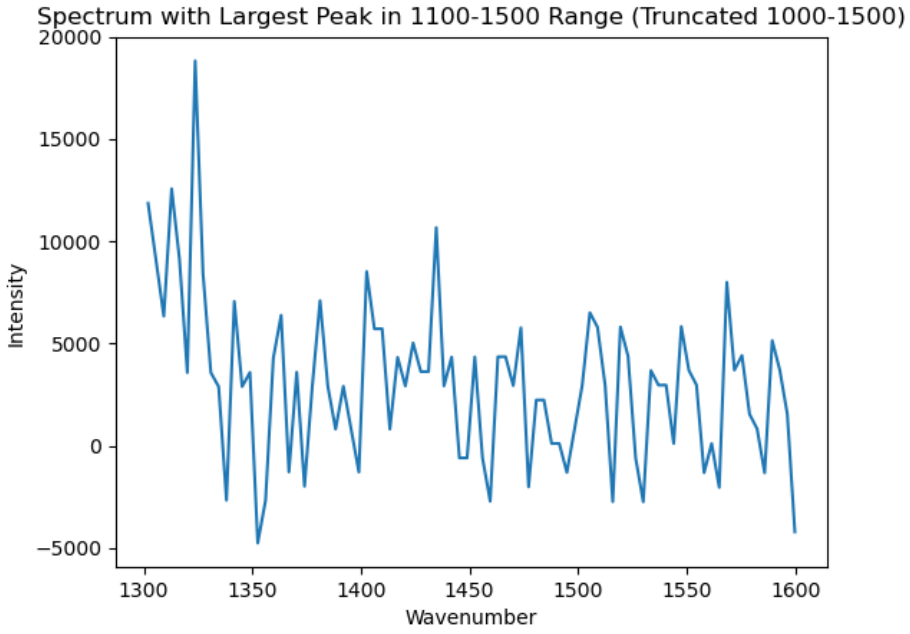

The above figures show the general optical characterization that occurred with the samples. First, we bulk scanned for particular hot spots (high plasmonic enhancement spots) within our corresponding gold structures, then we zoomed in and background subtracted the Raman signals for these structures. The bulk scan is evidently shown by the first image in this section. Now the second and third figures correspond to that sample's hot spot begin illuminated under a 750 nm laser and a 650 nm LED. These were done to show the corresponding plasmonic enhancement of the azobenzene treated samples. This is where the experiment hit a roadblock as we didn't see very significant enhancement with the LED (although it is nonzero, observed at wavelengths of approximately 1300, 1450, and 1575), and the leader at 750 nm was photobleaching the Raman enhanced signal of the azobenzene.

5.3 Theoretical Results

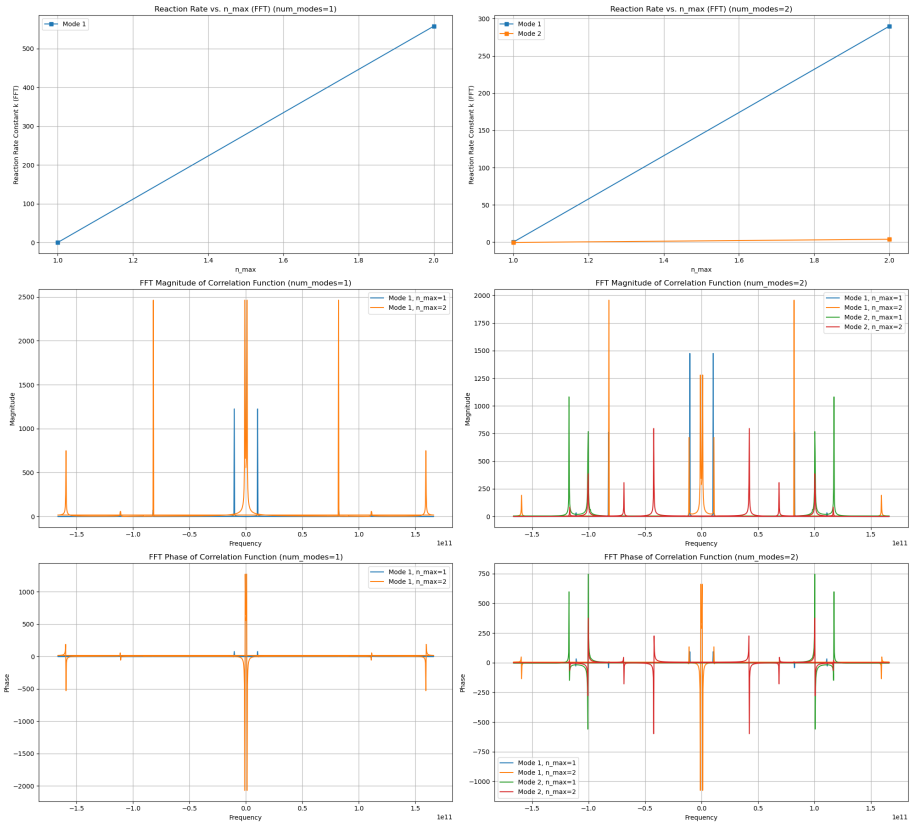

Figure 1: Results of the FFT analysis.

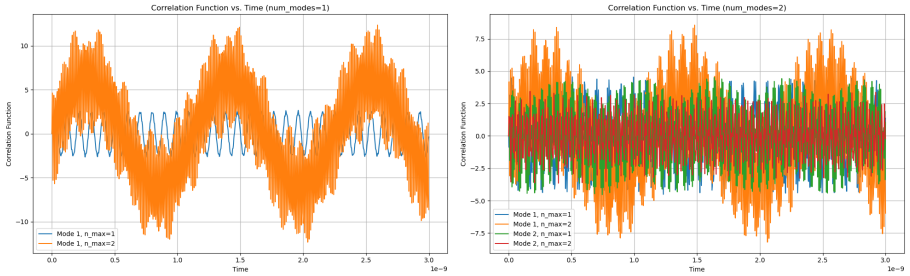

Figure 2: Results of the FFT analysis.

These plots were all calculated numerically via various Python codes. This analysis indicates that if one were able to modulate the number of plasmons

within the cavity inhabiting specific modes, that they would observe non-linear and qualitatively, destructively interfering transition rate behavior for the switching of the azobenzene molecule. This is a very interesting proposition, which needs experimental verification via the eventual completion of this research.

5.4 Future Work

Future work will focus on analyzing the differences in reaction rates due to differing plasmonic modes and plasmon numbers on the transition/reaction rates of azobenzene molecules. The photoswitching dynamics of the azobenzene molecules under plasmonic excitation will be investigated using Raman spectroscopy. The experimental results will then be compared to the theoretical predictions to validate the model and gain further insights into the plasmon-enhanced molecular switching process.

6 Conclusion

This research combines theoretical modeling and experimental nanofabrication to investigate the plasmon-enhanced photoswitching of azobenzene molecules. A non-equilibrium theoretical model has been developed to predict the reaction rates under plasmonic excitation, considering both weak and strong coupling regimes. Experimentally, we have successfully fabricated plasmonic nanostructures and characterized their optical properties. Future work will involve functionalizing these structures with azobenzene and utilizing Raman spectroscopy to probe the switching dynamics. The combination of theoretical modeling and experimental validation aims to provide a comprehensive understanding of plasmon-enhanced molecular switching, with potential applications in optical data storage, molecular electronics, and biosensing.

7 Acknowledgments

I would like to acknowledge Professor Scherer, Chiyoung Hwang, and Richard Smith for their extensive guidance in this project.

References

[1] S. A. Maier, "Plasmonics: Fundamentals and Applications," Springer Science Business Media, 2007.

[2] M. I. Stockman, "Nanoplasmonics: Past, Present, and Glimpse into Future," Optics Express, vol. 19, no. 22, pp. 22029-22106, 2011.

[3] M. L. Brongersma, N. J. Halas, and P. Nordlander, "Plasmon-induced Hot Carrier Science and Technology," Nature Nanotechnology, vol. 10, no. 1, pp. 25-34, 2015.

[4] H. Wei, Z. Wang, X. Tian, M. Käll, and H. Xu, "Nanoscale Optical Trapping and Directional Manipulation of Gold Nanorods," Nature Communications, vol. 4, no. 1, pp. 1-7, 2013.

[5] H. M. D. Bandara and S. C. Burdette, "Photoisomerization in Different Classes of Azobenzene," Chemical Society Reviews, vol. 41, no. 5, pp. 1809-1825, 2012.

[6] A. A. Beharry and G. A. Woolley, "Azobenzene Photoswitches for Biomolecules," Chemical Society Reviews, vol. 40, no. 8, pp. 4422-4437, 2011.

[7] K. A. Willets and R. P. Van Duyne, "Localized Surface Plasmon Resonance Spectroscopy and Sensing," Annual Review of Physical Chemistry, vol. 58, pp. 267-297, 2007.

[8] B. Y. Zheng, H. Zhao, A. Manjavacas, M. McClain, P. Nordlander, and N. J. Halas, "Distinguishing between Plasmon-induced and Photoexcited Carriers in a Device Geometry," Nature Communications, vol. 6, no. 1, pp. 1-7, 2015.

[9] Y. Tanimura, "Nonequilibrium reaction rate theory: Formulation and implementation within the hierarchical equations of motion approach," The Journal of Chemical Physics, vol. 153, no. 2, p. 020901, 2020.